International Journal of Biological Macromolecules 233 (2023) 123528

Contents lists available at ScienceDirect

International Journal of Biological Macromolecules

journal homepage: www.elsevier.com/locate/ijbiomac

Label-free biosensing of lignans for therapeutics using engineered model surfaces

Beatrix Péter [a,*], Barbara Majoros [a], Sándor Kurunczi [a], Andrea Violetta Ács [a], Inna Szekacs [a], Szilvia Bősze [b,c], Gábor M. Kovács [d,e], Imre Boldizsár [d,f], Robert Horvath [a,*]

[a] Nanobiosensorics Group, Research Centre for Energy Research, Institute for Technical Physics and Materials Science, Konkoly-Thege u 29-33, 1121 Budapest, Hungary
[b] MTA-ELTE Research Group of Peptide Chemistry, Eötvös Loránd Research Network (ELKH), Institute of Chemistry, Eötvös Loránd University, 1117 Budapest, Hungary
[c] National Public Health Center, Albert Flórián út 2-6, 1097 Budapest, Hungary
[d] Department of Plant Anatomy, Institute of Biology, Eötvös Loránd University, 1117 Budapest, Hungary
[e] Plant Protection Institute, Centre for Agricultural Research, ELKH, Budapest, Hungary
[f] Department of Pharmacognosy, Semmelweis University, Üllői út 26, 1085 Budapest, Hungary

ARTICLE INFO

Keywords:
Label-free biosensor
Engineered model surface
Lignans
Human serum albumin
Binding affinity
Kinetics

ABSTRACT

The label-free interaction analysis of macromolecules and small molecules has increasing importance nowadays, both in diagnostics and therapeutics. In the blood vascular system, human serum albumin (HSA) is a vital globular transport protein with potential multiple ligand binding sites. Characterizing the binding affinity of compounds to HSA is essential in pharmaceutics and in developing new compounds for clinical application. Aryltetralin lignans from the roots of *Anthriscus sylvestris* are potential antitumor therapeutic candidates, but their molecular scale interactions with specific biomolecules are unrevealed. Here, we applied the label-free grating-coupled interferometry (GCI) biosensing method with a polycarboxylate-based hydrogel layer with immobilized HSA on top of it. With this engineered model surface, we could determine the binding parameters of two novel aryltetralin lignans, deoxypodophyllotoxin (DPT), and angeloyl podophyllotoxin (APT) to HSA. Exploiting the multi-channel referencing ability, the unique surface sensitivity, and the throughput of GCI, we first revealed the specific biomolecular interactions. Traditional label-free kinetic measurements were also compared with a novel, fast way of measuring affinity kinetics using less sample material (repeated analyte pulses of increasing duration (RAPID)). Experiments with well-characterized molecular interactions (furosemide to carbonic-anhydrase (CAII) and warfarin, norfloxacin to HSA) were performed to prove the reliability of the RAPID method. In all investigated cases, the RAPID and traditional measurement gave similar affinity values. In the case of DPT, the measurements and relevant modeling suggested two binding sites on HSA, with dissociation constant values of $K_{d1} = 1.8 \pm 0.01$ μM, $K_{d2} = 3 \pm 0.02$ μM. In the case of APT, the experiments resulted in $K_{d1} = 9 \pm 1.7$ μM, $K_{d2} = 28 \pm 0.3$ μM. The obtained binding values might suggest the potential medical application of DPT and APT without further optimization of their binding affinity to HSA. These results could be also adapted to other biomolecules and applications where sample consumption and the rapidity of the measurements are critical.

1. Introduction

Certain plants can be used for medical applications due to the accumulation of special bioactive compounds majority representing the so-called secondary metabolites [1]. These compounds might be beneficial to human health, because of their anti-inflammatory or anticancer (antiproliferative) effects, among others [1]. Lignans are a large group of polyphenol-type secondary metabolites, many of which can potentially be used for medicinal purposes. Some classes of them are now receiving increased interest because there is growing evidence that the consumption of lignan-rich food can decrease the risk of certain types of cancer [2]. Among lignan-producing plants, *Anthriscus sylvestris* (L.) Hoffm. (cow parsley) is of primary importance due to the accumulation of antiproliferative podophyllotoxin derivatives in its root. This herbaceous perennial plant is common in most temperate regions, offering an easily available source of lignans. The main secondary metabolites in its roots are the aryltetralin lignans deoxypodophyllotoxin (DPT) and [3–5] angeloyl podophyllotoxin (APT) [6] (Fig. 1). These two lignans are

* Corresponding authors.
E-mail addresses: peter.beatrix@ek-cer.hu (B. Péter), horvath.robert@ek-cer.hu (R. Horvath).

https://doi.org/10.1016/j.ijbiomac.2023.123528
Received 16 November 2022; Received in revised form 24 January 2023; Accepted 30 January 2023
Available online 2 February 2023

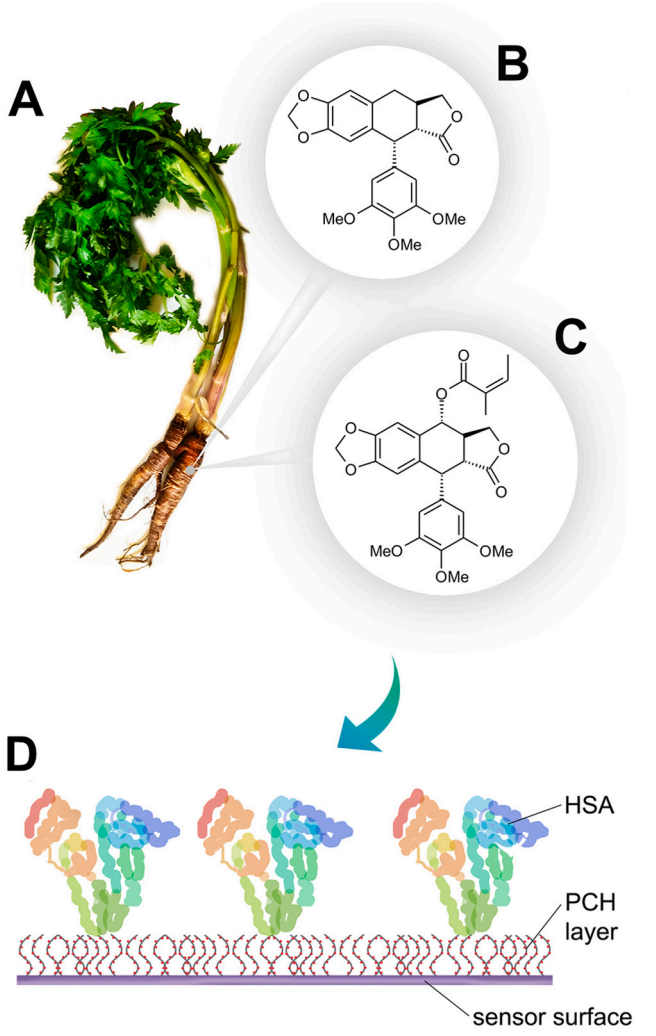

Fig. 1. The plant *Anthriscus sylvestris* (A) and chemical structures of the lignans deoxypodophyllotoxin (DPT) (B), and angeloyl podophyllotoxin (APT) (C) isolated from its root. These compounds are presented to the polycarboxylate-based hydrogel layer (PCH) with immobilized HSA on top of it (D).

valuable antiproliferative natural metabolites [6–8] and are also lead compounds for the development of antitumor agents [9]. Highlighting the importance of studying these types of compounds, two related podophyllotoxin derivatives, Etoposide and Teniposide, also become approved medications for the treatment of various tumors [9]. Thus, aryltetralin lignans have become the subject of extensive research [2].

Our research aimed to explore the binding properties of DPT and APT isolated from *A. sylvestris* to human serum albumin (HSA). This macromolecule is synthesized by the liver, and it is the most abundant protein in human blood plasma with a molecular weight of 66.5 kDa [10,11]. Active substances can be transported by HSA, it can also penetrate the blood-brain barrier [12,13]. Only the unbound fraction of a drug is capable of diffusing out of the vasculature and into the target tissue [12,13]. Therefore, interaction with HSA influences the absorption, distribution, metabolism, and excretion of small molecules [12,14]. Furthermore, HSA also transports hormones and fatty acids as well, buffers pH, and maintains oncotic pressure, among others [10,11]. Due to the relevance of transport functions of HSA, it is especially important to reveal the binding properties of newly developed agents or natural compounds to this protein during the development of next-generation drug delivery platforms. Thus, it is especially suited to study small molecule interactions in a real-time and label-free manner [15].

A novel type of biosensors, especially in combination with engineered surfaces for *in situ* kinetic analysis, has increasing importance not only in point-of-care diagnostics but also in the fast screening of medical applications [16–18]. Among others, optical sensor systems are especially promising, offering reliable and sensitive analysis down to the levels of ions [17,19–22].

In this work, we used grating-coupled interferometry (GCI) [17,18,23] to perform the biomolecular interaction analysis and to quantify binding kinetics. GCI is a hybrid phase-shifting Mach–Zehnder optical waveguide interferometer, which can present several advantages over other optical biosensor techniques [17,18,23–25]. In a typical GCI device, two light beams are coupled into a planar optical waveguide through two grating regions, representing the sensing and the reference beams. The phase shift caused by adsorption on the waveguide is precisely measured and analyzed using phase modulation. It is worth noting that it has a leading level of sensitivity superior to surface plasmon resonance (SPR) (reliable kinetics below 1 pg/mm^2, noise level < 0.01 pg/mm^2) [23,26]. Additional advantages are the crude sample robustness and the reliable microfluidics, normally achieved with plate-based assays only.

Thus, due to its performance, high-throughput setup, and excellent sensitivity, the GCI technique is an especially suitable tool in several research and development areas. It has found a broad range of applications for example in drug discovery [27], cancer research [28], characterization of natural active agent–protein interactions [23], and plant biology [29–36]. It was even well-suited to reveal the kinetic interactions of Ni(II) ions (52 Da) with Ni-specific genetically engineered proteins [17,18].

The scope of this study consists in comparing two measurement methods of the GCI system, the traditional kinetic measurement protocol and the newly developed Repeated Analyte Pulses of Increasing Duration (hereafter RAPID) *in situ* kinetic interaction analysis mode [37]. Moreover, we first determine the binding parameters of DPT and APT to HSA. To prove the reliability of the new method, the binding affinity of the sulfonamide-type diuretic agent furosemide to carbonic-anhydrase (CAII) was measured as a gold-standard reference [38]. For further comparison, the binding parameters of norfloxacin and warfarin to HSA were also investigated, having known binding parameters from previous studies [39–44]. Norfloxacin is a well-known fluoroquinolone antibiotic compound used mainly to treat urinary tract and gynecological infections and inflammation of the prostate gland [39–41]. Warfarin is a small-molecule anticoagulant agent used for preventing deep vein thrombosis, pulmonary embolism, and stroke [43,44]. All of these results prove the reliability of the novel RAPID assay, which offers faster results from less sample material. The obtained DPT–HSA and APT–HSA binding parameters suggest strong binding affinity and give important information on the potential further medical applications of these novel compounds.

2. Materials and methods

2.1. Materials and reagents

Roots of *Anthriscus sylvestris* were collected from two different locations in May 2020. Sample collection locations were near Budapest (47.527508, 18.954185 and 47.561571, 18.989130). The root samples were lyophilized on the day of collection. The voucher specimens of the dried samples are deposited in the Department of Plant Anatomy, Eötvös Loránd University, Budapest, Hungary.

Phosphate buffered saline (PBS) + 2 % dimethyl sulfoxide (DMSO, Sigma Aldrich) buffer continuously flowed over the sensor surface (running buffer). Human serum albumin (HSA, Sigma Aldrich) was dissolved in acetate buffer (10 mM, pH = 5). Deoxypodophyllotoxin (DPT) and angeloyl podophyllotoxin (APT) were isolated from the root of *A. sylvestris* as described below. Compounds were dissolved in 50 mM DMSO with PBS, and further diluted with PBS + 2 % DMSO. Fig. 1A shows the plant itself and the chemical structures of the isolated

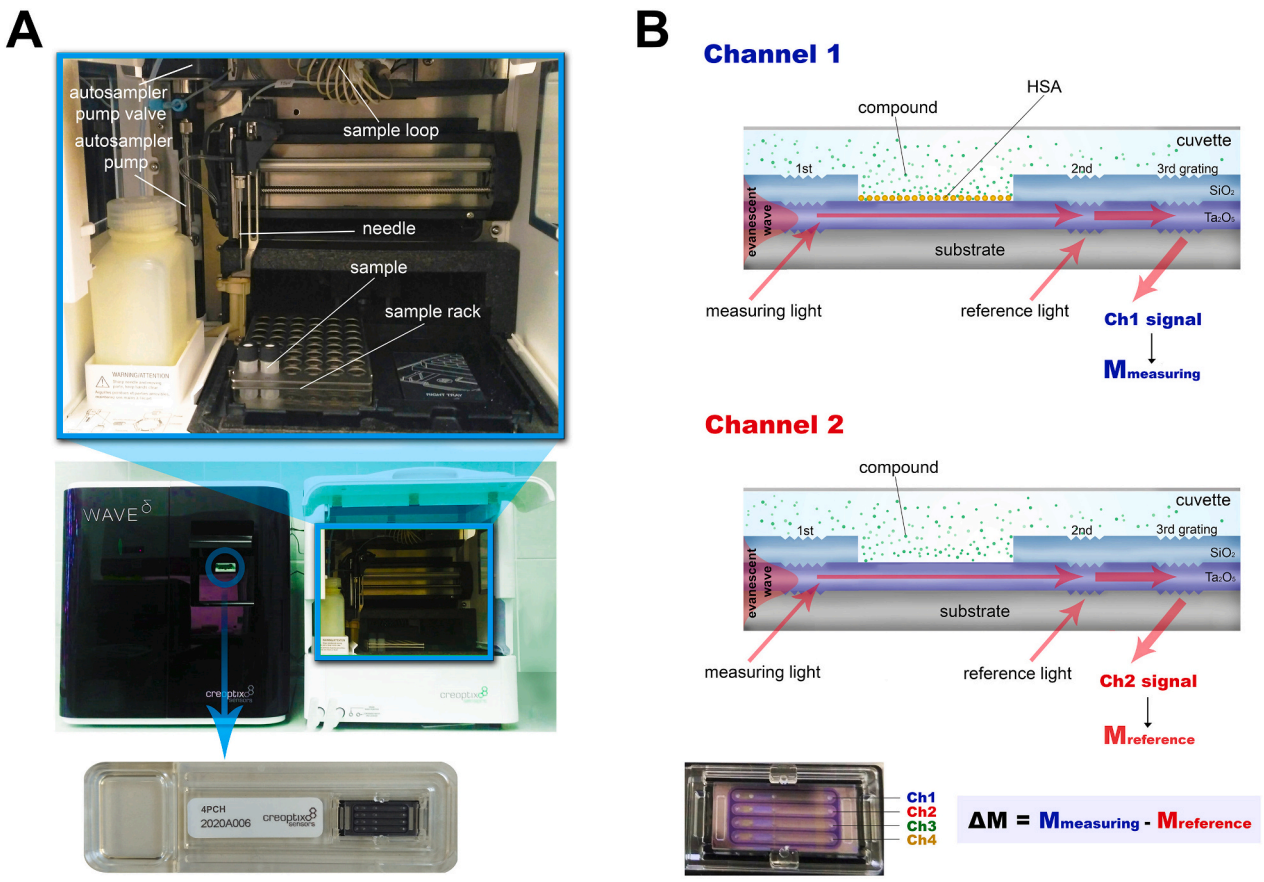

Fig. 2. The GCI instrument and the biosensor chip with 4 channels. A. Photo of the GCI device. Its interior part is magnified with a light blue frame. Here, the components (autosampler pump valve, autosampler pump, needle, sample rack) of the autosampler system and their layout are shown. The instrument applies a sensor chip (bottom part). B. The sensor chips used in the instrument have four channels (bottom left corner); minimum one for measuring the interaction between the immobilized bioreceptor and the analyte (measuring channel, *channel 1*) and one for subtracting the channel 1 signal by a reference signal (reference channel, *channel 2*). In our case, HSA (or CAII) was immobilized on the measuring channel. The reference channel was also activated by EDC/NHS and then passivated by ethanolamine, but remained untreated by HSA. The figure is based on our previous work [23].

compounds (Fig. 1B and C). These compounds are presented to the engineered model surface with immobilized HSA (Fig. 1D).

Furosemide (Sigma Aldrich) is an inhibitor of the carbonic-anhydrase enzyme (CAII, Sigma Aldrich), that can bind to the CAII immobilized previously to the chip according to the manufacturer's recommendations. Norfloxacin and warfarin were purchased from Sigma Aldrich.

2.2. Extraction of deoxypodophyllotoxin (DPT) and angeloyl podophyllotoxin (APT)

Solvents applied in the extraction, isolation, and analysis of compounds, such as acetonitrile, distilled water, formic acid, and methanol (Reanal, Hungary), were all of the analytical reagent grades of the highest purity available.

Lyophilized and pulverized root tissues of *A. sylvestris* (500.0 mg) were extracted with 20 mL of methanol in 50 mL screw-capped vials at 60 °C for 30 min. The insoluble, centrifuged material was subsequently re-extracted two times in the same way. The combined supernatants were dried by a standard vacuum rotary evaporator at 45 °C. Dried extracts were dissolved in 2.0 mL of methanol for the preparative high-performance liquid chromatography (HPLC) isolation of DPT and APT.

2.3. Preparative high-performance liquid chromatography

A Pharmacia LKB HPLC (Uppsala, Sweden) system (2248 pumps, VWM 2141 UV detector) was connected to a preparative HPLC column: Gemini NX-C18 (5 μm), 25 × 1 cm (Phenomenex, Torrance, CA, USA). Eluents: eluent A, 0.1 % *v*/v formic acid, eluent B, acetonitrile:0.1 % v/v formic acid (80:20, v/v). Gradient: 0.0 min, 30 % B; 50.0 min, 100 % B (linear gradient); 55.0 min, 100 % B (isocratic); flow rate: 5.0 mL/min; column temperature: ambient. Aliquots (500 μL) of the extracts (2.0 mL) were consecutively injected (four times) and the corresponding fractions containing the same compounds were combined and dried (by a vacuum rotary evaporator at 45 °C). Aliquots of the dried isolated compounds (DPT and APT) were dissolved in methanol to confirm their structures by analytical HPLC.

2.4. Compounds identification methods

To identify DPT and APT, analytical high-performance liquid chromatography (HPLC) hyphenated with ultraviolet (UV) spectrophotometry and high-resolution Orbitrap mass spectrometry (HRMS) were used.

A Dionex Ultimate 3000 UHPLC system (3000RS diode array detector (DAD), TCC-3000RS column thermostat, HPG-3400RS pump, SRD-3400 solvent rack degasser, WPS-3000TRS autosampler), connected to an Orbitrap Q Exactive Focus Mass Spectrometer equipped with electrospray ionization (ESI) (Thermo Fischer Scientific, Waltham, MA, USA) was used for the identification of isolated compounds. The HPLC separations were performed on a Gemini NX-C18 (3 μm), 150 × 3 mm (Phenomenex, Torrance, CA, USA) The eluents were the same as described above. Gradient: 0.0 min, 20 % B; 15.0 min, 90 % B (linear gradient); 19.0 min, 90 % B (isocratic); flow rate: 0.4 mL/min; column temperature: 25 °C; injected volume: 3.0 μL. The ESI source was

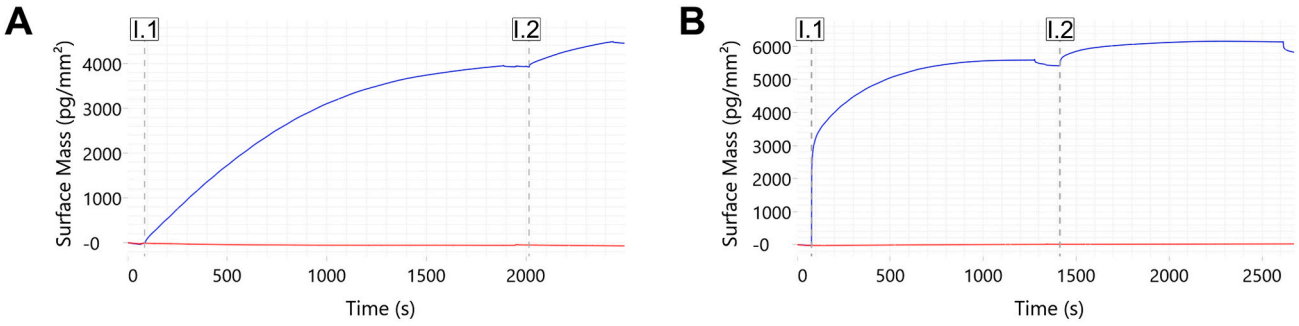

Fig. 3. Kinetic curves of the immobilization process of CAII (A) and HSA (B). The blue curve represents the signal of the measuring channel, while the red one shows the signal of the reference channel. In both cases, there were 2 cycles in the immobilization process. "I.1" with a grey dashed line represents the first, while "I.2" is the second injection.

operated in positive ionization mode. Operation parameters were optimized automatically by the built-in software as follows: spray voltage, 3500 V (+); capillary temperature 256 °C; sheath-, auxiliary- and spare-gases (N2): 47.50, 11.25, and 2.25 arbitrary units, respectively. The resolution of the full scan was 70,000. Scanning range: 100–1000 *m/z* units. UV spectra were recorded between 230 and 600 nm. The purity of compounds was determined by analyzing their HPLC-UV chromatograms.

2.5. Label-free kinetic measurements

The *in situ* monitoring of the binding events was performed using the WAVE Delta instrument (Creoptix AG, Switzerland, Fig. 2A) and WAVEchips with 4 fluidic channels (Fig. 2A bottom part and Fig. 2B) [17]. The instrument has a temperature-controlled autosampler system which enables the measurement of several samples in one measurement set [17,23].

After chip conditioning with borate buffer (0.1 M sodium borate pH 9.0, 1 M NaCl), subsequent injections of running buffer (0.2× PBS) were performed (startup cycles) to stabilize the baseline signal. The standard EDC/NHS (1-ethyl-3-(3-dimethylaminopropyl)carbodiimide hydro chloride/N-hydroxysuccinimide) coupling chemistry was used to covalently immobilize CAII or HSA onto the measuring channel.

10 μg/mL CAII was immobilized onto the carboxylated 4PCP (quasi planar polycarboxylate with covalent functionalization through –COOH group) surface at a high R_{max} level, resulting in an immobilized mass of above 4000 pg/mm^2 (Fig. 3A). During this immobilization step, 50 mM NaH_2PO_4 was used as a running buffer (pH = 5.6); finally, the activated chip surface was blocked with 1 M ethanolamine hydrochloride, pH = 8.0.

HSA was immobilized onto the polycarboxylate-based hydrogel layer on the measuring channel of 4PCH (thick hydrogel polycarboxylate with covalent functionalization through –COOH group, in the case of DPT and APT (Fig. 1D)) or 4PCP (norfloxacin, warfarin) chip at 1 mg/mL concentration in 10 mM sodium acetate buffer, pH 5. Then, the chip surface was blocked using 1 M ethanolamine hydrochloride, pH 8.0. The reference channel was activated by EDC/NHS and then passivated by ethanolamine, but remained untreated by HSA providing the reference signal (without HSA treatments, Fig. 3B). The resulting kinetic curves of the immobilization processes are shown in Fig. 3.

2.6. Traditional and RAPID (repeated analyte pulses of increasing duration) kinetic assays

In the case of furosemide – CAII measurement, PBS buffer +3 % DMSO was used as the running buffer. Furosemide working solution (100 μM) was prepared from 1 mM stock, using 3 dilutions and the dilution factor was 10. The RAPID method was used for the kinetic measurement, which uses pulses of analyte at a single concentration for the increased duration.

The covalently grafted HSA amount was at a surface density of 11,809 pg/mm^2. The kinetic series was preceded by 5–10 startups. Compounds were dissolved in 50 mM DMSO, then we diluted the solution with DMSO-free running buffer (Sörensen buffer +300 mM NaCl) to 1 mM and further diluted with Sörensen +300 mM NaCl +2 % DMSO (running buffer).

Traditional kinetics measurements were performed with a dilution series where the highest concentration was 306 μM, using 10 dilutions and the dilution factor was 3 in the case of DPT, and the highest concentration was 200 μM, using 10 dilutions and the dilution factor was 2 in the case of APT. Each solution was injected twice. To correct the bulk refractive index, DMSO calibration with different concentrations of

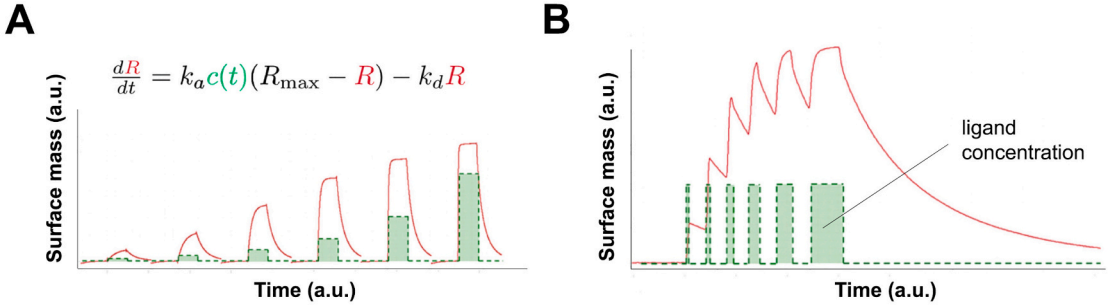

Fig. 4. Schematic kinetic curves by traditional and RAPID kinetics. A. In a typical assay with traditional kinetics, the analyte is flowed at increasing concentrations, with uniform duration. In every cycle, the injected concentration (ci) is fixed but c(t) is a function of time for the whole series (green). R is the sensorgram response, proportional to the mass of the bound analyte (red), and R_{max} is the highest response value. The model fitting provides estimates for the parameters. B. In the RAPID assay, the series contains only one cycle with only one association phase. This phase is interrupted by dissociation portions and a final dissociation phase. Model fitting is simpler because it can be done with the dissociation segments only, and this method requires less sample as well (no need for concentration series). [37]. This figure is based on the work of Kartal et al. [37].

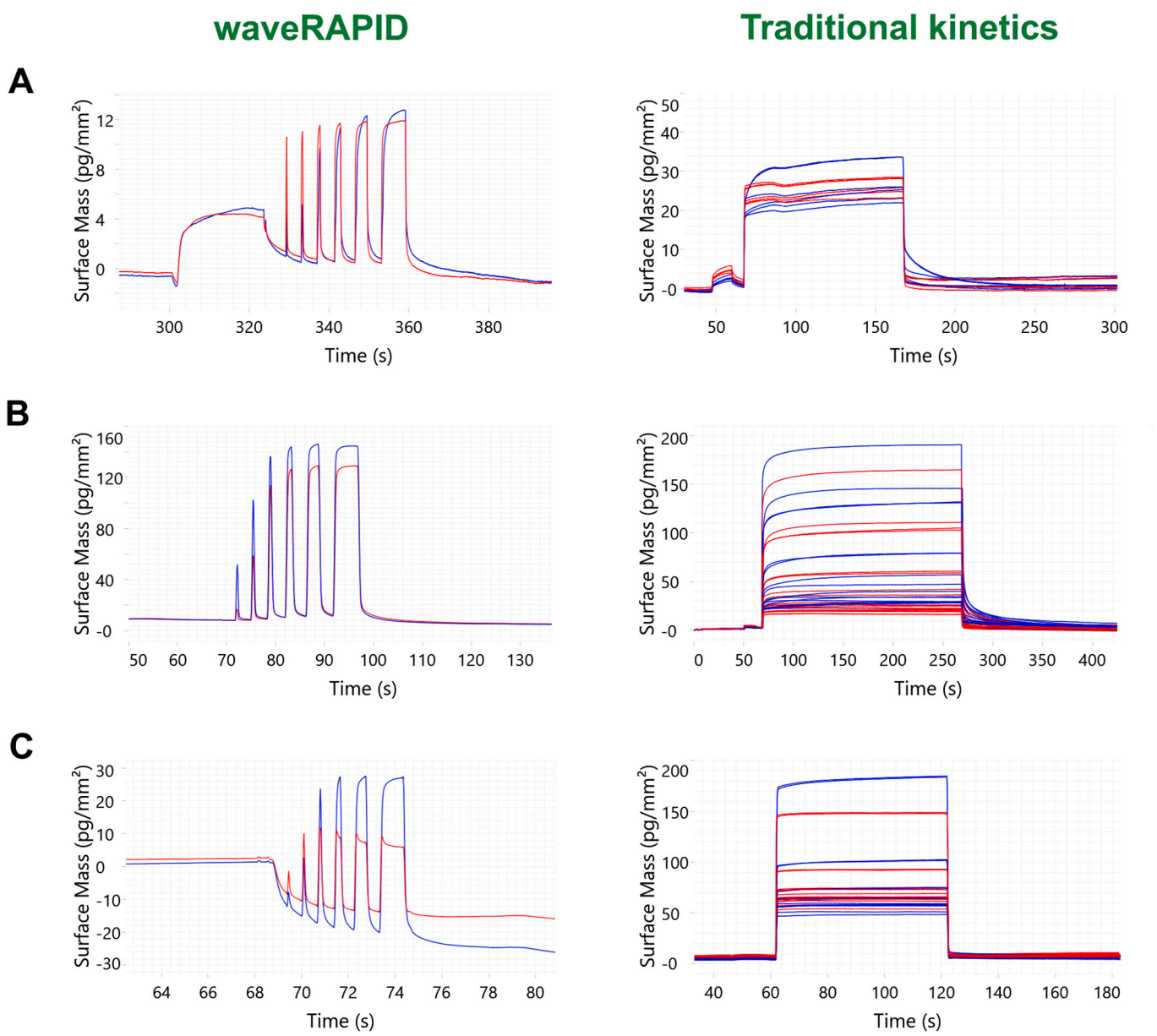

Fig. 5. The kinetic curves of furosemide (A), norfloxacin (B), warfarin (C) obtained by RAPID (curves on the left side) and traditional kinetics (curves on the right side). The blue curves are the measuring signals, and the red ones are the reference signals.

DMSO solutions was additionally performed. The need for this correction originates from the fact that the reference channel does not have the ligand-protein and, therefore, is more sensitive to the changes in the refractive index of the solution (also called the missing volume effect).

In the case of RAPID measurements, the dilution series was performed with the highest concentration of 10 μM. In both cases, the analysis of the given data was carried out using the WAVEcontrol 4.5.13. evaluation software.

The kinetic data were evaluated with two different models. The first model supposes only one compound-binding site on the HSA (in the evaluation program given as "1:1 kinetic"). The other one considers two binding sites with different affinities (in the evaluation program given as a "heterogeneous ligand"). Both the equilibrium curves and the kinetic curves were applied to define the K_d values.

3. Results and discussion

3.1. Traditional and RAPID kinetics

In the traditional ligand binding assay, the analyte is injected at increasing concentrations, with uniform duration in each case [37]. The model fitting provides estimates for the parameters (K_a, K_d, and R_{max}) of the ordinary differential equation (ODE) for the one-to-one binding that best explains the data in all segments of the time series. In the RAPID assay, the series contains a single cycle with just one association phase that is interrupted by dissociation portions and a final longer dissociation phase [37]. Thus, the model fitting can be done with the dissociation segments. In contrast to traditional, multicycle kinetics measurements, the novel RAPID generates a pulsating concentration profile by injecting the analyte at the same concentration, multiple times and with increased duration (Fig. 4) [37].

Therefore, RAPID injects a single concentration, but pulses the sample over the sensing surface at increasing durations. So the kinetics

Table 1
Mass spectrometry (MS) data of isolated compounds, determined by high-performance liquid chromatography (HPLC) high-resolution Orbitrap-MS using positive ionization mode.

Compound name	Formula	Detected ion	Measured mass (*m/z*)	Calculated mass (*m/z*)	Mass error (ppm)[a]
Deoxypodophyllotoxin (DPT)	$C_{22}H_{22}O_7$	$[M + H]^+$	399.14319	399.14383	−1.602
		$[M + NH_4]^+$	416.16956	416.17038	−1.967
Angeloyl podophyllotoxin (APT)	$C_{27}H_{28}O_9$	$[M + H]^+$	497.17941	497.18061	−2.411
		$[M + NH_4]^+$	514.20636	514.20716	−1.552
		$[M\text{-angelic acid}+H]^{+b}$	397.12750	397.12818	−1.711

[a] Differences between the measured and calculated masses (*m/z*) of ions varied between −1.552 ppm and −2.411 ppm, confirming the molecular formula of compounds.
[b] Characteristic fragment ion, generated from angeloyl podophyllotoxin by in-source fragmentation (*i.e.*, by fragmentation in the ion source).

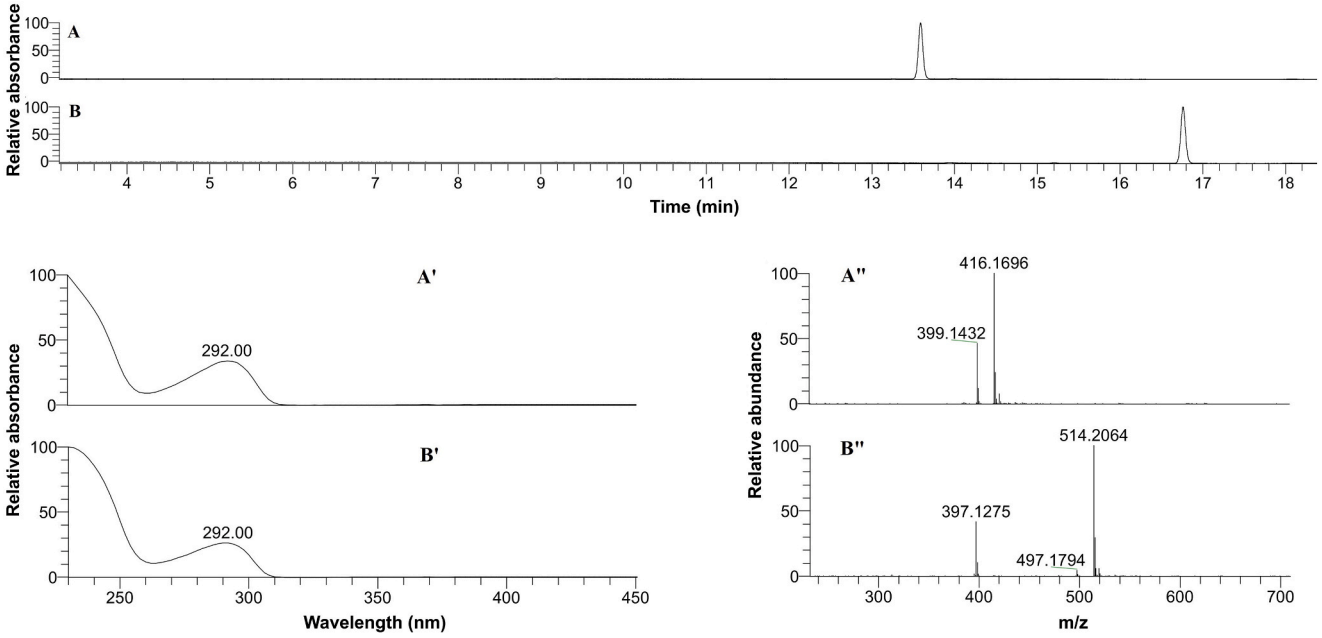

Fig. 6. High-performance liquid chromatography ultraviolet spectrophotometry (HPLC-UV) separations of the isolated deoxypodophyllotoxin (A), and angeloyl podophyllotoxin (B) (detected at 292 nm) and the corresponding UV spectra (A', B') and high-resolution mass spectra (HRMS, generated by positive ionization mode) (A", B") of these compounds.

can be derived from a single well without the requirement of serial dilutions, thus this is a time- and sample-saving, simpler method for detecting interactions of various molecules.

The measurement kinetic curves with both assays are plotted in Fig. 5 in the case of furosemide (Fig. 5A), norfloxacin (Fig. 5B), and warfarin (Fig. 5C). The figure emphasizes the different signals recorded at the reference and measurement channels to eliminate the signals of nonspecific binding.

3.2. Identifying the isolated compounds

The isolated compounds can be identified using the molecular formula (Table 1) and UV spectra (Fig. 6) identical to those of the known metabolites of *A. sylvestris*, DPT, and APT, respectively [5–7]. Cations formed with ammonium ions and protons can be detected in the mass spectra of both compounds (Fig. 6, panels A", B", Table 1).

The molecular formulas of compounds ($C_{22}H_{22}O_7$ and $C_{27}H_{28}O_9$), which were calculated from the *m/z* values of these ions, correspond to the lignans DPT and APT (Table 1). A high-intensity signal of the ion *m/z* 397.1275 can be observed in the mass spectra of APT due to the in-source fragmentation (*i.e.*, fragmentation in the ion source) of this compound (Fig. 6, panel B"), providing evidence of the existence of the angeloyl unit in APT (Table 1).

3.3. Dissociation constant values of the compounds and the proteins determined by RAPID and traditional kinetics methods

The furosemide measurements, which were obtained through both the RAPID and traditional methods, resulted in dissociation constant (K_d) values in the same range with almost the same numerical values: K_d values of 6 ± 1.3 and 4 ± 0.2 μM were determined, respectively, by employing the 1:1 kinetic fit in both cases (see Fig. 7A). Prior literature value for the furosemide binding to CAII is $K_d = 1 \pm 0.2$ μM [38], so we can conclude that our results, which were received by the two kinetic methods of GCI, are reliable and comparable.

Considering the norfloxacin binding to HSA, comparable K_d values were determined by the RAPID ($K_{d1} = 468 \pm 2.3$ μM, $K_{d2} = 651 \pm 4.6$ μM) and traditional ($K_{d1} = 310 \pm 2.2$ μM, $K_{d2} = 664 \pm 2.3$ μM) methods using the heterogeneous fit in both cases (Fig. 7B). These data are in good agreement with the literature results on the norfloxacin-HSA binding using surface plasmon resonance (SPR, $K_d = 980$ μM [39]), confirming that the new results received by the two independent methods of GCI are reliable and comparable. Note, however, the binding of norfloxacin to HSA has been characterized previously with significantly lower values using fluorescence, isothermal titration calorimetry (ITC), and circular dichroism (CD) measurements ($K_d = 16.7$–33.6 μM) [40,41]. We believe that the different results might be caused by the surface immobilization of HSA in the case of our GCI and previous SPR

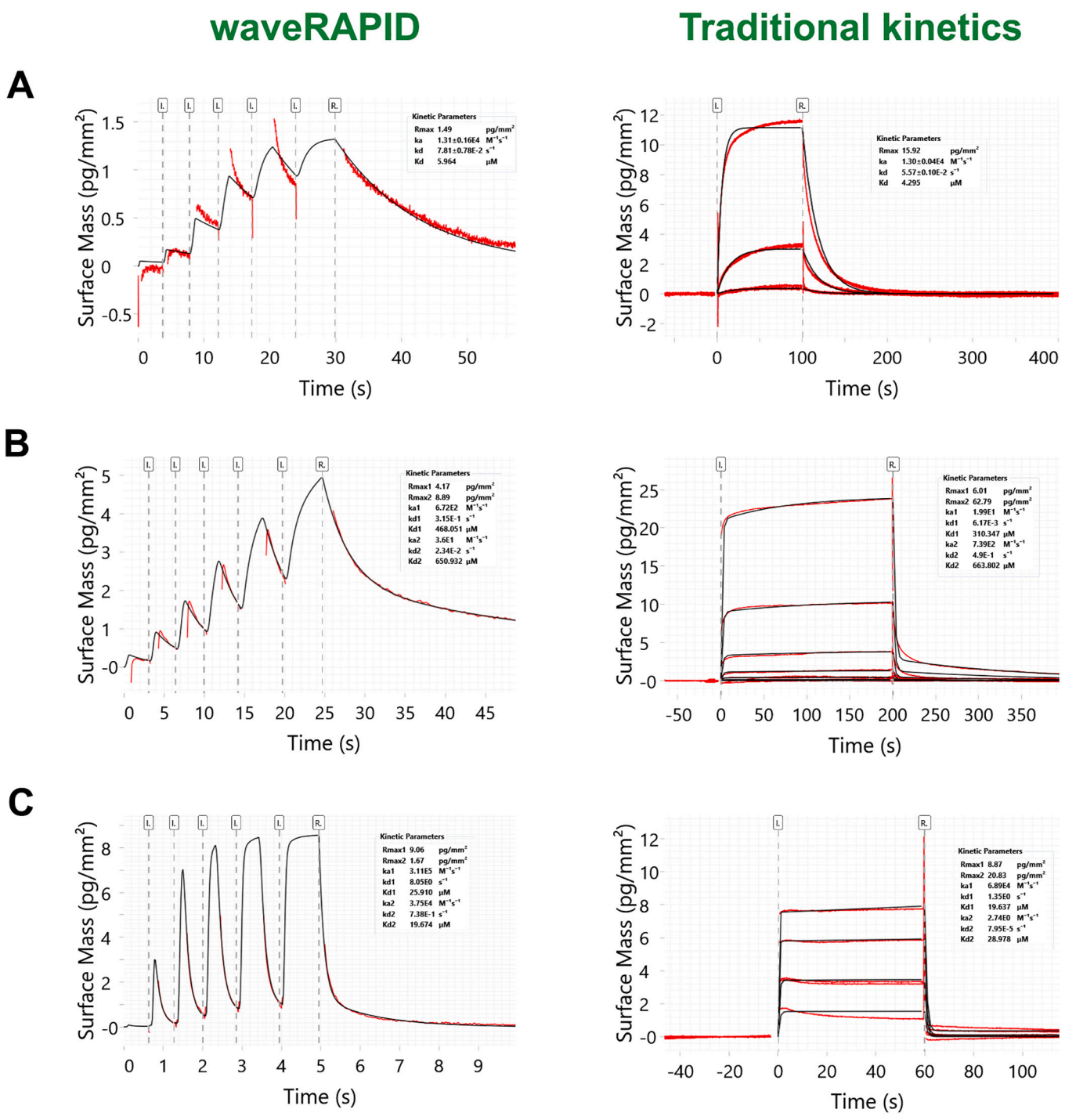

Fig. 7. The measured and fitted kinetic curves of furosemide (A), norfloxacin (B), warfarin (C) obtained by RAPID (curves on the left side) and traditional kinetics (curves on the right side). "I." with grey dashed lines represents the injections, and "R." shows the rinses. The red lines represent the measurement kinetic curves, and the black lines are the fitted curves. The received kinetic parameters shown in the graphs are summarized in Table 2.

measurements. Surface immobilization is not required in fluorescence, CD, and ITC affinity measurements. Similar observations regarding the effect of covalent immobilization were reported in the case of ion binding of genetically engineered protein layers [17].

The warfarin experiments resulted in K_d values in the same range; with RAPID, the $K_{d1} = 26 \pm 0.1$ μM, $K_{d2} = 19.7 \pm 0.08$ μM, while $K_{d1} = 20 \pm 0.2$ μM, $K_{d2} = 29 \pm 0.2$ μM with the traditional kinetics from the heterogeneous kinetic modeling in both cases (Fig. 7C). Binding of warfarin (and other small molecules, such as diazepam and ibuprofen) to HSA occur at relatively well-defined regions on the protein. The two well-characterized binding regions are the warfarin-azapropazone site (located in the IIA subdomain) and the indole-benzodiazepine site (located in the IIIA subdomain) of HSA [45,46]. Furthermore, Oester and co-workers reported primary and secondary binding sites for warfarin [42]. The literature data are in the range of K_d = 3–37 μM [43–45,47–50], however, a study by Rich et al. mentions a value of 273 μM as well [47]. Furthermore, another study [44] also declares a higher value for K_{d2} = 284.6–398.3 μM (in the case of 0 % and 5 % ethanol, respectively). Of note, this equilibrium dialysis data also suggested two warfarin binding sites on HSA, similar to our data, but with one order of

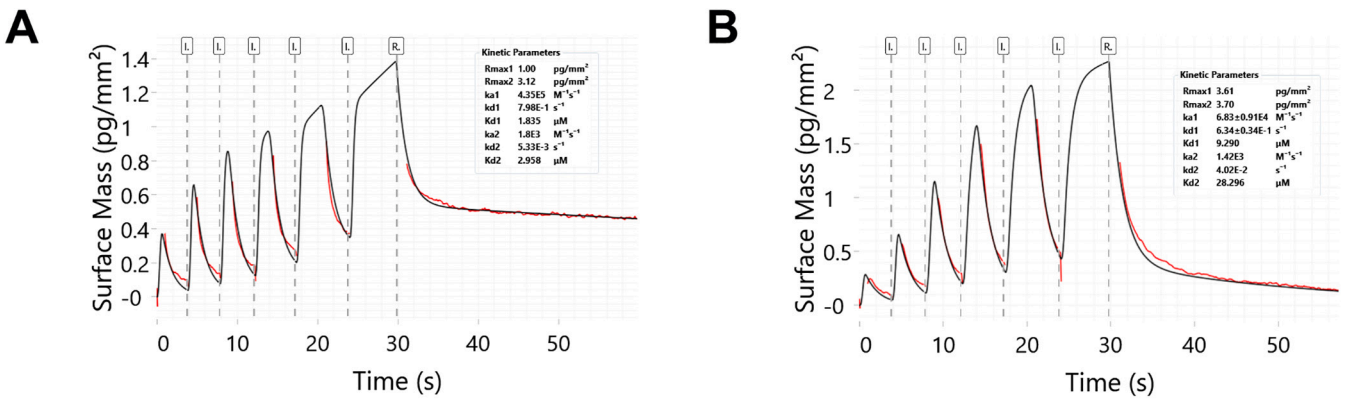

Fig. 8. The measured and fitted kinetic curves of DPT (A), and APT (B) obtained by RAPID. "I." with grey dashed lines represents the injections, and "R." shows the rinses. The red lines represent the measurement kinetic curves, and the black lines are the fitted curves. The received kinetic parameters shown in the graphs are summarized in Table 3.

magnitude larger K_{d2} value for the low-affinity binding site.

Our experimental results and the affinity values found in the literature are comparable, and in all cases, the RAPID and traditional measurements gave similar affinity values. Therefore, one can conclude that the novel RAPID kinetic analysis method gives reliable results in the case of known drug-active substances.

After summarizing the results of the active substances with already known binding parameters, we turn to the isolated natural compounds with unknown binding affinities.

In the case of DPT, 1:1 kinetic modeling did not result in acceptable fits. Employing the heterogeneous modeling, RAPID measurements resulted in K_d values of $K_{d1} = 1.8 \pm 0.01$ µM, $K_{d2} = 3 \pm 0.02$ µM. (Fig. 8A). The obtained values are in asimilar range, but the relatively close values of the two individual binding sites raise the hypothesis of one type of binding site on HSA with varying binding environments. It is important to note; the immobilization of proteins might cause a slight change in the binding site affinity due to the steric constraints caused by the covalent immobilization, which could lead to the appearance of two binding sites with slightly different affinity values [17]. A similar effect was observed in case of our APT experiments. APT data were also well-fitted by the heterogeneous model. By employing the RAPID assay, the $K_{d1} = 9 \pm 1.7$ µM, $K_{d2} = 28 \pm 0.3$ µM were obtained (Fig. 8B). Table 3 summarizes the obtained affinity values for DPT-HSA and APT-HSA interactions.

The obtained relatively strong binding values might suggest the potential clinical application of DPT and APT without further optimization of their binding affinity to HSA. The obtained affinities are especially useful when the slow release of the drugs is needed, and HSA is not only considered as a transport molecule, but also acts as a buffer to prolong drug action [12–14].

Table 2
Summary of the results of furosemide, norfloxacin and warfarin received by the different types of assays.

Compound	Ligand	RAPID kinetics	TRADITIONAL kinetics
Furosemide (331 Da)	CAII	$K_d = 6 \pm 1.3$ µM $k_a = 1.3 \times 10^4$ M^{-1} s^{-1} $k_d = 7.8 \times 10^{-2}$ s^{-1} (1:1 kinetics)	$K_d = 4 \pm 0.2$ µM $k_a = 1.3 \times 10^4$ M^{-1} s^{-1} $k_d = 5.6 \times 10^{-2}$ s^{-1} (1:1 kinetics)
Norfloxacin (319 Da)	HSA	$K_{d1} = 468 \pm 2.3$ µM, $K_{d2} = 651 \pm 4.6$ µM $k_{a1} = 6{,}7 \times 10^2$ M^{-1} s^{-1}, $k_{a2} = 3.6 \times 10^1$ M^{-1} s^{-1} $k_{d1} = 3.2 \times 10^{-1}$ s^{-1}, $k_{d2} = 2.3 \times 10^{-2}$ s^{-1} (heterogeneous)	$K_{d1} = 310 \pm 2.2$ µM, $K_{d2} = 664 \pm 2.3$ µM $k_{a1} = 2$ M^{-1} s^{-1}, $k_{a2} = 7.4 \times 10^2$ M^{-1} s^{-1} $k_{d1} = 6.2 \times 10^{-3}$ s^{-1}, $k_{d2} = 4.9 \times 10^{-1}$ s^{-1} (heterogeneous)
Warfarin (308 Da)	HSA	$K_{d1} = 26 \pm 0.1$ µM, $K_{d2} = 19.7 \pm 0.08$ µM $k_{a1} = 3.1 \times 10^5$ M^{-1} s^{-1}, $k_{a2} = 3.8 \times 10^4$ M^{-1} s^{-1} $k_{d1} = 8$ s^{-1}, $k_{d2} = 7.4 \times 10^{-1}$ s^{-1} (heterogeneous)	$K_{d1} = 20 \pm 0.2$ µM, $K_{d2} = 29 \pm 0.2$ µM $k_{a1} = 6.9 \times 10^4$ M^{-1} s^{-1}, $k_{a2} = 2.7$ M^{-1} s^{-1} $k_{d1} = 1.4$ s^{-1}, $k_{d2} = 8 \times 10^{-5}$ s^{-1} (heterogeneous)

Table 3
Summary of the obtained affinity data for DPT and APT.

Ligand	**DPT** (398 Da)	**APT** (496 Da)
HSA	$K_{d1} = 1.8 \pm 0.01$ µM, $K_{d2} = 3 \pm 0.02$ µM $k_{a1} = 4.4 \times 10^5$ M^{-1} s^{-1}, $k_{a2} = 1.8 \times 10^3$ M^{-1} s^{-1} $k_{d1} = 8 \times 10^{-1}$ s^{-1}, $k_{d2} = 5.3 \times 10^{-3}$ s^{-1} (heterogeneous)	$K_{d1} = 9 \pm 1.7$ µM, $K_{d2} = 28 \pm 0.3$ µM $k_{a1} = 6.8 \times 10^4$ M^{-1} s^{-1}, $k_{a2} = 1.4 \times 10^3$ M^{-1} s^{-1} $k_{d1} = 6.3 \times 10^{-1}$ s^{-1}, $k_{d2} = 4 \times 10^{-2}$ s^{-1} (heterogeneous)

4. Conclusions

In this work, we determined the interaction of HSA protein with two novel type of aryltetralin lignans deoxypodophyllotoxin (DPT), and angeloyl podophyllotoxin (APT) from *A. sylvestris*, using a highly sensitive label-free optical biosensor (GCI). HSA is known as the most important transport protein in human plasma, with remarkable ligand binding capacity. The processes of binding various bioactive compounds with HSA are studied very extensively. The affinity of bioactive compounds to HSA strongly influences their pharmacokinetic profile, related to permeability through tissue barriers and the *in vivo* distribution. There are rapidly establishing equilibria between the HSA and the binding compounds and their complexes, and these can be characterized by the thermodynamic association (K_a) or dissociation (K_d) constants. Many important properties and kinetic data are influenced by the magnitudes of these values.

The applied technique enables the collection of reference-corrected kinetic data about molecular binding events. The present work also compared two assays; the traditional kinetics and the newly introduced RAPID kinetic analysis method. The novel RAPID assay uses traditional equipment and techniques, but offers several advantages due to a design that is superior to that of traditional assays; it saves measurement time, is more cost-effective, and requires less amount of samples. The increased throughput can improve hit quality and shorten cycle times considerably in early-stage drug discovery. The additional measurements with already known drugs were also performed; the binding values of norfloxacin and warfarin to HSA and that of furosemide to CAII were also analyzed and compared to literature values

[38–41,43–45,47–50]. We found that both assays are suitable for determining drug interactions with HSA, but the RAPID assay significantly facilitates the measurement processes. Of note, the RAPID measurements gave reliable K_d values in all investigated cases, but we have found some discrepancies in the kinetic rate constants (see Table 2). This effect should be investigated further in later works.

HSA binding of bioactive compounds is well-recognized and the implications for compounds' action *in vivo* have been fully appreciated. HSA regarding its high concentration, controls the free compound concentration in plasma and compartments in equilibrium with plasma, thereby effectively attenuating the potency *in vivo*. Therefore, characterization of binding to HSA and obtaining the binding constants are essential for any new bioactive compounds, and candidate drugs. By employing the novel RAPID assay, we have determined the affinity values of two new natural compounds DPT and APT and obtained binding constants in the μM range, meaning strong binding to HSA.

The presented methods could be extended to other types of ligands and analytes. The increased throughput of RAPID measurements would shorten cycle times considerably in early-stage drug discovery, which is a rather important aspect in pharmaceutics and the development of new therapeutic or diagnostic agents.

Declaration of competing interest

The authors declare that they have no known competing financial interests or personal relationships that could have appeared to influence the work reported in this paper.

Data availability

Data will be made available on request.

Acknowledgements

We would like to thank Alexandra Vörös, Kinga Tóth, Krisztina Borbély, and Tamás Gerecsei for helping in the initial experiments, and Edward Fitzgerald (Malvern Panalytical (Creoptix AG)) for his expertise and useful advice in the grating coupled interferometry technique. This research was funded by the Hungarian Academy of Sciences [Lendület (Momentum) Program], the National Research, Development, and Innovation Office (NKFIH) [ERC_HU, PD 131543 (B·P) and KKP_19 Programs] and grant OTKA (number 135712, 142904) and TKP2022-EGA-04 program. S.B., G.M.K., and I.B. acknowledge the support of the ELTE Thematic Excellence Programme supported by the Hungarian Ministry for Innovation and Technology and ELTE Thematic Excellence Programme 2020 supported by the National Research, Development and Innovation Office (TKP2020-IKA-05). S.B., G.M.K., and I.B. thank the support of grant EFOP-1.8.0-VEKOP-17-2017-00001.

References

[1] B. Péter, I. Boldizsár, G.M. Kovács, A. Erdei, Z. Bajtay, A. Vörös, J.J. Ramsden, I. Szabó, S. Bősze, R. Horvath, Natural compounds as target biomolecules in cellular adhesion and migration: from biomolecular stimulation to label-free discovery and bioactivity-based isolation, Biomedicines 9 (2021), https://doi.org/10.3390/biomedicines9121781.

[2] B. Botta, G. Monache, D. Misiti, A. Vitali, G. Zappia, Aryltetralin lignans: chemistry, pharmacology and biotransformations, Curr. Med. Chem. 8 (2012) 1363–1381, https://doi.org/10.2174/0929867013372292.

[3] A. Koulman, R. Bos, M. Medarde, N. Pras, W.J. Quax, A fast and simple GC MS method for lignan profiling in Anthriscus sylvestris and biosynthetically related plant species, Planta Med. 67 (2001) 858–862, https://doi.org/10.1055/s-2001-18849.

[4] A. Koulman, S. Batterman, F.M.S. Van Putten, R. Bos, W.J. Quax, Lignan profiles of indoor-cultivated Anthriscus sylvestris, Planta Med. 69 (2003) 959–961, https://doi.org/10.1055/s-2003-45110.

[5] O. Hendrawati, H.J. Woerdenbag, P.J.A. Michiels, H.G. Aantjes, A. Van Dam, O. Kayser, Identification of lignans and related compounds in Anthriscus sylvestris by LC-ESI-MS/MS and LC-SPE-NMR, Phytochemistry 72 (2011) 2172–2179, https://doi.org/10.1016/j.phytochem.2011.08.009.

[6] E.K. Seo, M.E. Wall, M.C. Wani, H. Navarro, R. Mukherjee, N.R. Farnsworth, A. D. Kinghorn, Cytotoxic constituents from the roots of tovomita brevistaminea, Phytochemistry 52 (1999) 669–674, https://doi.org/10.1016/S0031-9422(99)00274-5.

[7] G.S. Jeong, O.K. Kwon, B.Y. Park, S.R. Oh, K.S. Ahn, M.J. Chang, W.K. Oh, J. C. Kim, B.S. Min, Y.C. Kim, H.K. Lee, Lignans and coumarins from the roots of Anthriscus sylvestris and their increase of caspase-3 activity in HL-60 cells, Biol. Pharm. Bull. 30 (2007) 1340–1343, https://doi.org/10.1248/bpb.30.1340.

[8] M. Khaled, Z.Z. Jiang, L.Y. Zhang, Deoxypodophyllotoxin: a promising therapeutic agent from herbal medicine, J. Ethnopharmacol. 149 (2013) 24–34, https://doi.org/10.1016/j.jep.2013.06.021.

[9] X. Zhang, K.P. Rakesh, C.S. Shantharam, H.M. Manukumar, A.M. Asiri, H. M. Marwani, H.L. Qin, Podophyllotoxin derivatives as an excellent anticancer aspirant for future chemotherapy: a key current imminent needs, Bioorg. Med. Chem. 26 (2018) 340–355, https://doi.org/10.1016/j.bmc.2017.11.026.

[10] T. Pappa, S. Refetoff, Thyroid Hormone Transport Proteins: Thyroxine-binding Globulin, Transthyretin, and Albumin, Elsevier, 2016, https://doi.org/10.1016/B978-0-12-809324-5.03494-5.

[11] G. Fanali, A. Di Masi, V. Trezza, M. Marino, M. Fasano, P. Ascenzi, Human serum albumin: from bench to bedside, Mol. Asp. Med. 33 (2012) 209–290, https://doi.org/10.1016/j.mam.2011.12.002.

[12] K.W. Lexa, E. Dolghih, M.P. Jacobson, A structure-based model for predicting serum albumin binding, PLoS One 9 (2014), https://doi.org/10.1371/journal.pone.0093323.

[13] V. Ramanathan, N. Vachharajani, Protein binding in drug discovery and development, in: Eval. Drug Candidates Preclin. Dev. Pharmacokinet. Metab. Pharm. Toxicol 00, 2010, pp. 135–167, https://doi.org/10.1002/9780470574898.ch6.

[14] F. Kratz, B. Elsadek, Clinical impact of serum proteins on drug delivery, J. Control. Release 161 (2012) 429–445, https://doi.org/10.1016/j.jconrel.2011.11.028.

[15] J. Fan, K. Gilmartin, S. Octaviano, F. Villar, B. Remache, J. Regan, Using human serum albumin binding affinities as a proactive strategy to affect the pharmacodynamics and pharmacokinetics of preclinical drug candidates, ACS Pharmacol. Transl. Sci. 5 (2022) 803–810, https://doi.org/10.1021/acsptsci.2c00115.

[16] P. Chandra, R. Prakash, Nanobiomaterial Engineering, Concepts and Their Applications in Biomedicine and Diagnostics, Springer, 2020. ISBN : 978-981-32-9839-2.

[17] H. Jankovics, B. Kovacs, A. Saftics, T. Gerecsei, É. Tóth, I. Szekacs, F. Vonderviszt, R. Horvath, Grating - coupled interferometry reveals binding kinetics and affinities of ni ions to genetically engineered protein layers, Sci. Rep. (2020) 1–11, https://doi.org/10.1038/s41598-020-79226-w.

[18] A. Saftics, S. Kurunczi, B. Peter, I. Szekacs, J.J. Ramsden, R. Horvath, Data evaluation for surface-sensitive label-free methods to obtain real-time kinetic and structural information of thin films: a practical review with related software packages, Adv. Colloid Interf. Sci. 294 (2021), https://doi.org/10.1016/j.cis.2021.102431.

[19] M.C. Estevez, M. Alvarez, L.M. Lechuga, Integrated optical devices for lab-on-a-chip biosensing applications, Laser Photonics Rev. 6 (2012) 463–487, https://doi.org/10.1002/lpor.201100025.

[20] B. Purohit, P.R. Vernekar, N.P. Shetti, P. Chandra, Biosensor nanoengineering: design, operation, and implementation for biomolecular analysis, Sensors Int. 1 (2020), 100040, https://doi.org/10.1016/j.sintl.2020.100040.

[21] J. Homola, S.S. Yee, G. Gauglitz, Surface plasmon resonance sensors: review, Sensors Actuators B Chem. 54 (1999) 3–15, https://doi.org/10.1016/S0925-4005(98)00321-9.

[22] K. Mahato, P.K. Maurya, P. Chandra, Fundamentals and commercial aspects of nanobiosensors in point-of-care clinical diagnostics, 3 Biotech 8 (2018), https://doi.org/10.1007/s13205-018-1148-8.

[23] B. Peter, A. Saftics, B. Kovacs, S. Kurunczi, R. Horvath, Oxidization increases the binding of EGCG to serum albumin revealed by kinetic data from label-free optical biosensor with reference channel, Analyst 145 (2020) 588–595, https://doi.org/10.1039/c9an01779h.

[24] P. Kozma, A. Hamori, K. Cottier, S. Kurunczi, R. Horvath, Grating coupled interferometry for optical sensing, Appl. Phys. B Lasers Opt. 97 (2009) 5–8, https://doi.org/10.1007/s00340-009-3719-1.

[25] D. Patko, B. Gyorgy, A. Nemeth, K.E. Szabó-Taylor, A. Kittel, E.I. Buzas, R. Horvath, Label-free optical monitoring of surface adhesion of extracellular vesicles by grating coupled interferometry, Sensors Actuators B Chem. 188 (2013) 697–701, https://doi.org/10.1016/j.snb.2013.07.035.

[26] https://www.malvernpanalytical.com/en/products/product-range/WAVE.

[27] W. Pitsawong, V. Buosi, R. Otten, R.V. Agafonov, A. Zorba, N. Kern, S. Kutter, G. Kern, R.A.P. Pádua, X. Meniche, D. Kern, Dynamics of human protein kinase aurora a linked to drug selectivity, elife 7 (2018) 1–30, https://doi.org/10.7554/eLife.36656.

[28] F. Andres, L. Iamele, T. Meyer, J.C. Stüber, F. Kast, E. Gherardi, H.H. Niemann, A. Plückthun, Inhibition of the MET kinase activity and cell growth in MET-addicted cancer cells by bi-paratopic linking, J. Mol. Biol. 431 (2019) 2020–2039, https://doi.org/10.1016/j.jmb.2019.03.024.

[29] U. Hohmann, J. Nicolet, A. Moretti, L.A. Hothorn, M. Hothorn, The SERK3 elongated allele defines a role for BIR ectodomains in brassinosteroid signalling, Nat. Plants 4 (2018) 345–351, https://doi.org/10.1038/s41477-018-0150-9.

[30] U. Hohmann, J. Santiago, J. Nicolet, V. Olsson, F.M. Spiga, L.A. Hothorn, M. A. Butenko, M. Hothorn, Mechanistic basis for the activation of plant membrane receptor kinases by SERK-family coreceptors, Proc. Natl. Acad. Sci. U. S. A. 115 (2018) 3488–3493, https://doi.org/10.1073/pnas.1714972115.

[31] S. Okuda, S. Fujita, A. Moretti, U. Hohmann, V.G. Doblas, Y. Ma, A. Pfister, B. Brandt, N. Geldner, M. Hothorn, Molecular mechanism for the recognition of sequencedivergent CIF peptides by the plant receptor kinases GSO1/SGN3 and GSO2, Proc. Natl. Acad. Sci. U. S. A. 117 (2020) 2693–2703, https://doi.org/10.1073/pnas.1911553117.

[32] S. Moussu, C. Broyart, G. Santos-Fernandez, S. Augustin, S. Wehrle, U. Grossniklaus, J. Santiago, Structural basis for recognition of RALF peptides by LRX proteins during pollen tube growth, Proc. Natl. Acad. Sci. U. S. A. 117 (2020) 7494–7503, https://doi.org/10.1073/pnas.2000100117.

[33] K. Lau, R. Podolec, R. Chappuis, R. Ulm, M. Hothorn, Plant photoreceptors and their signaling components compete for COP 1 binding via VP peptide motifs, EMBO J. 38 (2019) 1–18, https://doi.org/10.15252/embj.2019102140.

[34] L. Lorenzo-Orts, U. Hohmann, J. Zhu, M. Hothorn, Molecular characterization of Chad domains as inorganic polyphosphate-binding modules, Life Sci. Alliance 2 (2019) 1–14, https://doi.org/10.26508/lsa.201900385.

[35] N.M. Doll, S. Royek, S. Fujita, S. Okuda, S. Chamot, A. Stintzi, T. Widiez, M. Hothorn, A. Schaller, N. Geldner, G. Ingram, A two-way molecular dialogue between embryo and endosperm is required for seed development, Science (80-.) 367 (2020) 431–435, https://doi.org/10.1126/science.aaz4131.

[36] P.J. Sandoval, J. Santiago, In vitro analytical approaches to study plant ligand-receptor INTeRactions1[Open], Plant Physiol. 182 (2020) 1697–1712, https://doi.org/10.1104/PP.19.01396.

[37] Ö. Kartal, F. Andres, M.P. Lai, R. Nehme, K. Cottier, waveRAPID—a robust assay for high-throughput kinetic screens with the creoptix WAVEsystem, SLAS Discov. 26 (2021) 995–1003, https://doi.org/10.1177/24725552211013827.

[38] G.A. Papalia, S. Leavitt, M.A. Bynum, P.S. Katsamba, R. Wilton, H. Qiu, M. Steukers, S. Wang, L. Bindu, S. Phogat, A.M. Giannetti, T.E. Ryan, V.A. Pudlak, K. Matusiewicz, K.M. Michelson, A. Nowakowski, A. Pham-Baginski, J. Brooks, B. C. Tieman, B.D. Bruce, M. Vaughn, M. Baksh, Y.H. Cho, M. De Wit, A. Smets, J. Vandersmissen, L. Michiels, D.G. Myszka, Comparative analysis of 10 small molecules binding to carbonic anhydrase II by different investigators using biacore technology, Anal. Biochem. 359 (2006) 94–105, https://doi.org/10.1016/j.ab.2006.08.021.

[39] X. Liu, D. Song, Q. Zhang, Y. Tian, Z. Liu, H. Zhang, Characterization of drug-binding levels to serum albumin using a wavelength modulation surface plasmon resonance sensor, Sensors Actuators B Chem. 117 (2006) 188–195, https://doi.org/10.1016/j.snb.2005.11.023.

[40] O. Azimi, Z. Emami, H. Salari, J. Chamani, Probing the interaction of human serum albumin with norfloxacin in the presence of high-frequency electromagnetic fields: fluorescence spectroscopy and circular dichroism investigations, Molecules 16 (2011) 9792–9818, https://doi.org/10.3390/molecules16129792.

[41] B.K. Paul, N. Ghosh, S. Mukherjee, Interplay of multiple interaction forces: binding of norfloxacin to human serum albumin, J. Phys. Chem. B 119 (2015) 13093–13102, https://doi.org/10.1021/acs.jpcb.5b08147.

[42] Y.T. Oester, S. Keresztes-Nagy, R.F. Mais, J. Becktel, J.F. Zaroslinski, Effect of temperature on binding of warfarin by human serum albumin, J. Pharm. Sci. 65 (1976) 1673–1677, https://doi.org/10.1002/jps.2600651127.

[43] R.A. O'Reilly, Interaction of the anticoagulant drug warfarin and its metabolites with human plasma albumin, J. Clin. Invest. 48 (1969) 193–202, https://doi.org/10.1172/JCI105968.

[44] C.E. Ha, C.E. Petersen, D.S. Park, K. Harohalli, N.V. Bhagavan, Investigations of the effects of ethanol on warfarin binding to human serum albumin, J. Biomed. Sci. 7 (2000) 114–121, https://doi.org/10.1007/BF02256617.

[45] H.S. Kim, I.W. Wainer, Rapid analysis of the interactions between drugs and human serum albumin (HSA) using high-performance affinity chromatography (HPAC), J. Chromatogr. B Anal. Technol. Biomed. Life Sci. 870 (2008) 22–26, https://doi.org/10.1016/j.jchromb.2008.05.029.

[46] U. Krach-Hansen, V.T.G. Chuang, M. Otagiri, Practical aspects of the ligand-binding and enzymatic properties of human serum albumin, Biol. Pharm. Bull. 25 (2002) 695–704, https://doi.org/10.1248/bpb.25.695.

[47] R.L. Rich, Y.S.N. Day, T.A. Morton, D.G. Myszka, High-resolution and high-throughput protocols for measuring drug/human serum albumin interactions using BIACORE, Anal. Biochem. 296 (2001) 197–207, https://doi.org/10.1006/abio.2001.5314.

[48] F.J. Diana, K. Veronich, A.L. Kapoor, Binding of nonsteroidal anti-inflammatory agents and their effect on binding of racemic warfarin and its enantiomers to human serum albumin, J. Pharm. Sci. 78 (1989) 195–199, https://doi.org/10.1002/jps.2600780304.

[49] I. Petitpas, A.A. Bhattacharya, S. Twine, M. East, S. Curry, Crystal structure analysis of warfarin binding to human serum albumin. Anatomy of drug site I, J. Biol. Chem. 276 (2001) 22804–22809, https://doi.org/10.1074/jbc.M100575200.

[50] A. Tatsumi, M. Kadobayashi, S. Iwakawa, Effect of ethanol on the binding of warfarin enantiomers to human serum albumin, Biol. Pharm. Bull. 30 (2007) 826–829, https://doi.org/10.1248/bpb.30.826.